The WFIRST coronagraph instrument: a major step in the exploration of sun-like planetary systems via direct imaging

Bertrand Mennesson, J. Debes, E. Douglas, B. Nemati, C. Stark, et al.

Bertrand Mennesson, J. Debes, E. Douglas, B. Nemati, C. Stark, J. Kasdin, B. Macintosh, M. Turnbull, M. Rizzo, A. Roberge, N. Zimmerman, K. Cahoy, J. Krist, V. Bailey, J. Trauger, J. Rhodes, L. Moustakas, M. Frerking, F. Zhao, I. Poberezhskiy, R. Demers, "The WFIRST coronagraph instrument: a major step in the exploration of sun-like planetary systems via direct imaging," Proc. SPIE 10698, Space Telescopes and Instrumentation 2018: Optical, Infrared, and Millimeter Wave, 106982I (1 August 2018); doi: 10.1117/12.2313861

SPIE.

Event: SPIE Astronomical Telescopes + Instrumentation, 2018, Austin, Texas, United States

The WFIRST Coronagraph Instrument: a major step in the exploration of Sun-like planetary systems via direct imaging

Bertrand Mennesson*[a], J. Debes[b], E. Douglas[c], B. Nemati[d], C. Stark[b], J. Kasdin[e], B. Macintosh[f], M. Turnbull[g], M. Rizzo[h], A. Roberge[h], N. Zimmerman[h], K. Cahoy[c], J. Krist[a], V. Bailey[a], J. Trauger[a], J. Rhodes[a], L. Moustakas[a], M. Frerking[a], F. Zhao[a], I. Poberezhskiy[a], R. Demers[a] and the WFIRST Coronagraph Science Investigation Teams

[a]Jet Propulsion Laboratory, California Institute of Technology, 4800 Oak Grove Drive, Pasadena, CA 9[1]109, USA; [b]Space Telescope Science Institute, Baltimore, MD 21218, USA; [c]Space, Telecommunications, Astronomy, and Radiation Laboratory, Department of Aeronautics and Astronautics, Massachusetts Institute of Technology, 77 Massachusetts Avenue, Cambridge, MA, USA; [d]University of Alabama, 301 Sparkman Dr., OPB400, Huntsville, AL 35899, USA; [e]Dept. of Mechanical and Aerospace Engineering Princeton University, Princeton, New Jersey 08544, USA; [f]Kavli Institute for Particle Astrophysics and Cosmology, Department of Physics, Stanford University, 382 Via Pueblo Mall, Stanford, CA USA; [g]SETI Institute, Carl Sagan Center for the Study of Life in the Universe, Off-Site: 2801 Shefford Drive, Madison, WI 53719, USA; [h]NASA Goddard Space Flight Center, 8800 Greenbelt Road, MD, 20771, USA

ABSTRACT

The Wide Field Infrared Survey Telescope (WFIRST) Coronagraph Instrument (CGI) will be the first high-performance stellar coronagraph using active wavefront control for deep starlight suppression in space, providing unprecedented levels of contrast and spatial resolution for astronomical observations in the optical. One science case enabled by the CGI will be taking visible images and (R~50) spectra of faint interplanetary dust structures present in the habitable zone of nearby sunlike stars (~10 pc) and within the snow-line of more distant ones (~20 pc), down to dust brightness levels commensurate with that of the solar system zodiacal cloud. Reaching contrast levels below 10^{-7} at sub-arcsecond angular scales for the first time, CGI will cross an important threshold in debris disks physics, accessing disks with low enough optical depths that their structure is dominated by transport mechanisms rather than collisions. Hence, CGI will help us understand how exozodiacal dust grains are produced and transported in low-density disks around mature stars. Additionally, CGI will be able to measure the brightness level and constrain the degree of asymmetry of exozodiacal clouds around individual nearby sunlike stars in the optical, at the ~3x solar zodiacal emission level. This information will be extremely valuable for optimizing the observational strategy of possible future exo-Earth direct imaging missions, especially those planning to operate at optical wavelengths as well, such as the Habitable Exoplanet Observatory (HabEx) and the Large Ultraviolet/Optical/Infrared Surveyor (LUVOIR).

Keywords: Exoplanets, high contrast imaging, space astronomy, coronagraphy, debris disks, exozodiacal light
*Bertrand.Mennesson@jpl.nasa.gov; phone 1 818 354-0494

1. INTRODUCTION

The Coronagraph instrument (CGI) on WFIRST will serve as a major technology demonstrator in preparation for future high contrast direct imaging missions dedicated to the spectral characterization of mature exoplanetary systems in reflected light and aiming to obtain optical spectra of rocky planets in the habitable zone (HabEx and LUVOIR concept studies). Indeed, CGI will demonstrate key technologies required for high contrast coronagraphy: autonomous ultra-precise (sub-nm) wavefront sensing and control, the use of large format (48x48) deformable mirrors in space, high contrast "broad-band" (>10% bandwidth) coronagraphic masks, operation of ultra-low dark current (~ 10^{-4} e^-/pix/s) photon counting detectors (EM CCDs) in a relevant space environment (L2 orbit), post-processing of broad-band images and integral field spectrograph data at unprecedented contrast levels (at least 30x better than currently demonstrated at <0.3" separations, see Figure 1). Beyond the demonstration of these individual technologies, CGI will validate the whole system level performance and end-to-end model predictions for conducting high contrast imaging from a space platform.

Space Telescopes and Instrumentation 2018: Optical, Infrared, and Millimeter Wave, edited by Makenzie Lystrup, Howard A. MacEwen, Giovanni G. Fazio, Proc. of SPIE Vol. 10698, 106982I
 · doi: 10.1117/12.2313861

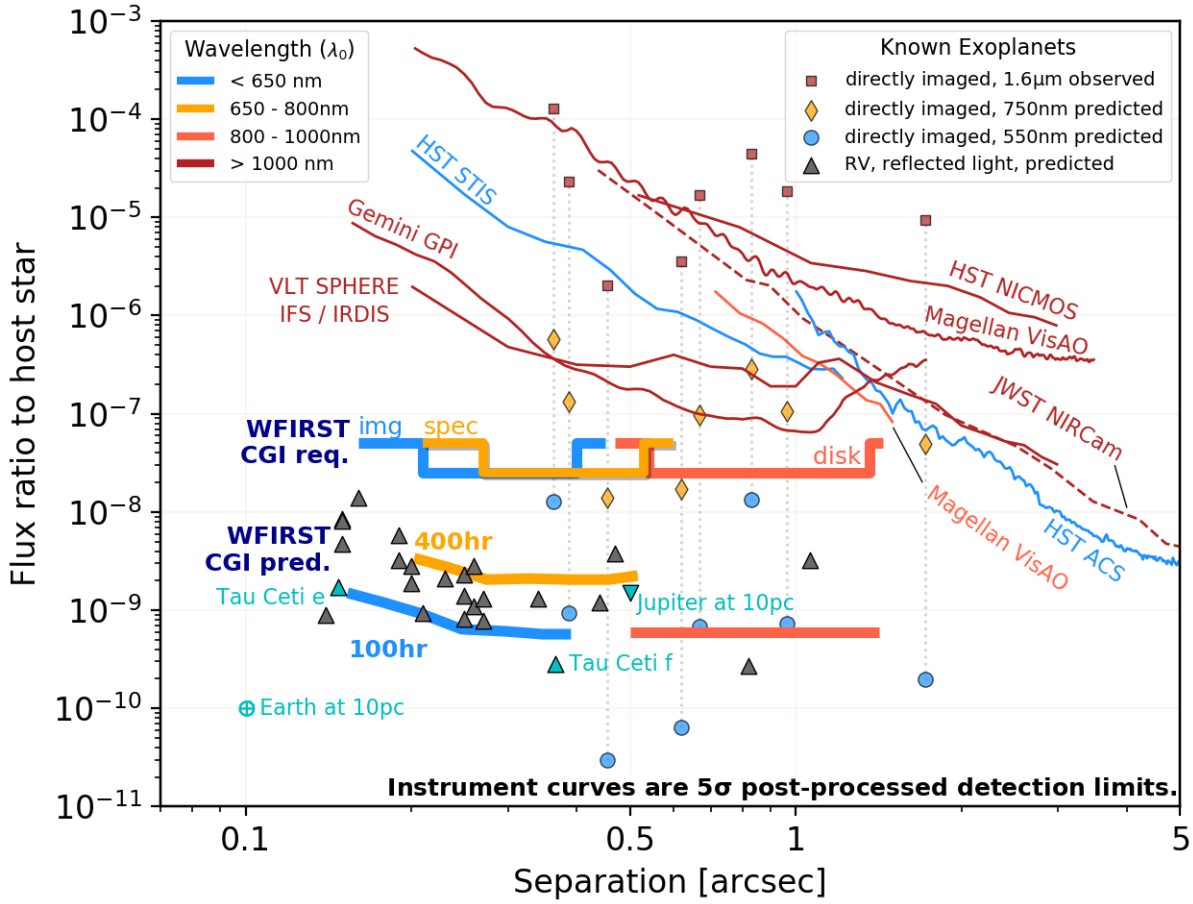

Figure 1: CGI baseline requirements and predicted CGI performance on a V=5 star, in the context of known giant planets and current instrumentation. The y-axis indicates the flux ratio between a planet and its host star (for individual planets) or between the dimmest source detectable at 5-sigma after post-processing (for instrument performance curves) and its host star. The x-axis is projected separation in arcseconds. Points and lines are color-coded by wavelength of observation. Solid and dashed lines are 5-sigma point source detection limits versus separation from the host star; these limits are calculated from post-processed data. The predicted performance for the future observatory, JWST, is plotted as a dashed line. Lines labeled "CGI pred." are performance predictions based on current-lab results. Black triangular points are estimated reflected light flux ratios for known gas giant radial velocity-detected (RV) planets at quadrature, with assumed geometric albedos of 0.5. Red squares are 1.6μm flux ratios of known self-luminous directly-imaged (DI) planets. Dotted lines connect each DI planet's known 1.6μm flux ratio to its predicted flux ratio at 750nm (yellow diamonds) or 550nm (blue circles), based on COND or BT-Settl planet evolutionary models. Cyan points represent the reflected light flux ratios of Earth and Jupiter at 10pc as well as super-Earths Tau Ceti e and f. Credit: Vanesssa Bailey (JPL).

It will improve and inform models about key engineering aspects (e.g. DM electronics, fine pointing control systems, precision mask mechanisms), disturbances in actual space environment (including those that affect the amplitude, temporal and spatial frequencies of observed wavefront drifts), in-orbit operations (autonomous starlight suppression systems, attitude maneuvers to enable differential imaging) and data calibration (application of advanced high contrast speckles subtraction algorithms, extraction of point source positions, fluxes and spectra from real astrophysical scenes, including all detector artifacts, and recorded at the relevant flux levels).

A successful CGI technology demonstration that meets the baseline technical requirements[46] ("BTRs") will have science capability. Figure 1 indicates the BTRs of CGI, expressed in terms of flux-ratio detection limits as a function of separation, as well as the prediction based on current laboratory results. Obviously, the quality and magnitude of potential CGI

scientific investigations will depend on the exact level of performance demonstrated during the on-orbit commissioning and CGI tech demonstration phase (predicted to be 3 months over the first 18 months of the mission). At the BTR performance level, visible images and spectra of self-luminous planets previously detected in the near-IR could be obtained, as well as images of debris disks ~100x fainter than those previously imaged by HST in scattered light (see section 4), and at smaller separations. If the demonstrated detection limit per resolution element is closer to a flux ratio of ~ 10^{-9}, as suggested by current lab-validated performance of WFIRST coronagraphs, wavefront control and detectors (Figure 1 "WFIRST CGI pred" curves), more ambitious science investigations will be possible. They include blind searches of mature giant planets seen in reflected light around nearby stars, optical spectra of mature Jupiter analogues previously detected by ground-based radial velocity (RV) observations, or the detection and spatial characterization of habitable zone dust (exozodiacal dust located in the inner part of debris disks) at ~3x the solar system density level. The focus of this paper is exozodiacal dust; we describe hereafter the scientific potential of CGI exozodiacal observations, and how they benefit future direct imaging missions.

2. WHAT IS (EXO)ZODIACAL DUST AND HOW DOES IT IMPACT EXOPLANET DIRECT IMAGING?

The solar system zodiacal cloud contains a population of small (~1–100 μm) warm dust grains located within the asteroid belt, extending from <0.1 AU to ~3.3 AU. The Cosmic Background Explorer (COBE) Diffuse Infrared Background Experiment (DIRBE) included measurements of the zodiacal light foreground from 1.25 to 240 μm, enabling modeling of its brightness distribution, grain size distribution, temperature, and optical depth radial profiles with high accuracy[1,2]. While the zodiacal cloud optical depth is only 10^{-7} at 1 AU and its total mass estimated to only a few 10^{-9} of Earth's mass—equivalent to an asteroid of 15 km in diameter—its spatially integrated flux dominates that of any planet in the solar system at any wavelength ranging from the optical to the mid-infrared (IR).

Zodiacal dust is believed to originate in asteroid collisions and the evaporation and/or break-up of comets as they approach the Sun. While some authors suggest that most of the observed dust is of cometary origin, e.g., created via spontaneous disruption of Jupiter family comets[4], the relative contribution of asteroids and comets is still under debate. Similarly, "exozodiacal" dust refers to the inner (separations of up to a few AU) warmer (> 200 K) part of circumstellar debris disks, where terrestrial planets form, and where we might see the signature of "exo-comets" and "exo-asteroids." Because zodiacal dust grain lifetimes are much shorter than stellar lifetimes, it is generally believed that exozodiacal dust must be regenerated[5] to be observed around main sequence stars. The inner brightness distribution of equivalent "exozodiacal" dust structures in debris disks around other mature stars is then expected to reflect present dust sources (comets, asteroids), as well as sinks (Poynting-Robertson drag, stellar radiation pressure), and perturbations (collisions, evaporation, planets), revealing some of the system's current dynamical state and formation history. In particular, bright exozodiacal disks may be the signposts of outer planets scattering numerous comets in the inner regions, similar to what happened during the solar system Late Heavy Bombardment[4,6].

But the presence of exozodiacal dust is really a double-edged sword for understanding exoplanet systems. Bright exozodiacal dust structures can provide key information about the dynamical processes at play in other planetary systems, but at the same time, they may degrade or inhibit the ability to directly image and spectrally characterize planets around other stars, particularly any faint Earth-like exoplanets orbiting in their habitable zone (HZ). Considering for instance a 4 m telescope viewing a Sun-Earth twin system at 10 pc at 60 deg inclination with an exact replica of the solar zodiacal cloud, the corresponding exozodiacal dust flux *per spatial resolution element* (PSF FWHM) is a few hundred times brighter than the Earth at 10 μm[7,8], and still ~3 times brighter than the Earth seen at quadrature in the visible[9]. A bright exozodiacal disk will contribute a higher background noise and increase the exposure time required for exoplanet direct detection. Realistic and optimized observing scenarios for exo-Earth direct-imaging missions[10] estimate that a factor of 10 increase in exozodiacal dust density level, e.g., from solar level (1 "zodi") to 10 times higher (10 "zodis"), reduces the exo-Earth yield of such missions by a factor of ~2. While manageable, this loss in sensitivity is still significant.

A potentially more problematic effect of bright exozodiacal emission is the creation of bright "clumps," regions of density enhancement trailing and leading the planet in its orbit, as predicted by disk-planet interaction models and actually observed in the solar system[1]. Simulations conducted in the case of an Earth analog embedded in exozodiacal clouds of different brightnesses[11] predict that at a level of 20 "zodis," local heterogeneities in the disk could be brighter than an exo-Earth and constitute important sources of confusion and false positives. The exact location and strength of exozodiacal clumps is expected to vary with planet mass, semi-major axis and outer dust characteristics such as density and typical grain size[12].

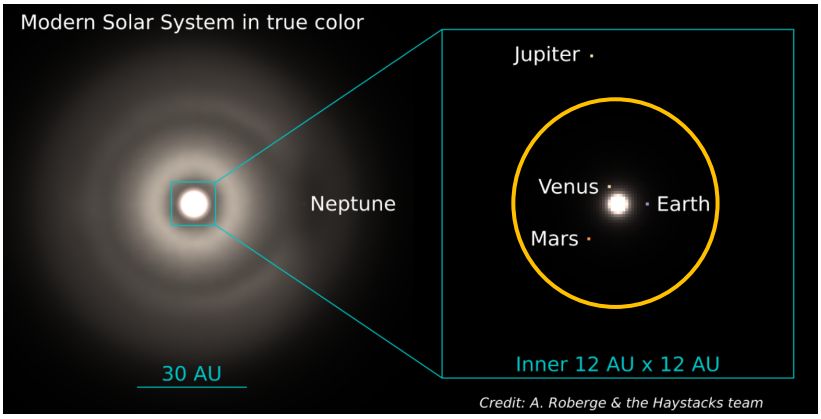

Figure 2: Model[3] of the solar system as viewed pole-on in the visible with a spatial resolution of 0.03 AU per pixel and the Sun "removed". *Left panel*: brightness scaling adjusted to highlight dust structures. *Right panel*: zoom-in of the inner region *with a steeper (non-linear)* brightness scaling revealing the Earth, Venus, and Mars. The solar zodiacal emission shown at the very center of the left panel arises from regions within the main asteroid belt, at the approximate distance represented by the yellow circle. Credit: Aki Roberge (NASA-GSFC) and the "Haystacks" team[3].

The main result is that exozodiacal clouds at density levels of ~20 solar zodis or more may generate bright enough clumps to preclude the direct detection of exo-Earths, or at least make data interpretation difficult, especially for systems seen at high inclination. In highly inclined systems, we must look through a much larger column of dust to see planets, including any cold dust in the system. Although one may think this cold dust would be negligibly faint due to the $1/r^2$ illumination factor, forward scattering of light by dust grains can partially counter this effect[13]. As a result, the surface brightness in an edge-on HZ can be dominated by dust physically located beyond a few AU instead of dust within the HZ[13]. It is therefore important to improve knowledge of exozodiacal disk brightness level and morphology—both per individual star and in a statistical sense—plays an important role for optimizing future space missions aiming at the characterization of Earth-like exoplanets, as recognized early on[11,14].

3. STATE OF KNOWLEDGE AND LIMITATIONS OF EXISTING FACILITIES

If exozodiacal clouds are similar to what is observed in the solar system, their spatially integrated flux—relative to the central star—is roughly 1,000 times brighter in the mid-IR than in the visible. For example, for a perfect solar system analog seen pole-on, the ratio of total zodiacal flux to stellar flux is $\sim 4\times10^{-5}$ at 10 μm, compared to only $\sim 4\times10^{-8}$ at V band[1]. This advantage in contrast is well known, and in the absence of a high-contrast visible space-based coronagraph, exozodiacal surveys have been primarily conducted in the mid-IR, either through space-based spectroscopic measurements, or through ground-based spatially resolved measurements.

Space-based infrared telescopes, such as the Infrared Astronomical Satellite (IRAS), the Infrared Space Observatory (ISO), and Spitzer all have a too small aperture to spatially separate the exozodiacal dust emitting region from the central star. They rely instead on spectral excess measurements, which require careful calibration and accurate subtraction of the model-dependent stellar spectral energy distribution. As a result, and because of the smaller relative flux contributed by HZ dust at shorter infrared wavelengths, Spitzer detection limits for exozodiacal disks are typically 100 zodis at 24 μm, and 1,000 zodis at 10 μm. Only a few warm excesses have been detected by Spitzer around mature stars above these detection thresholds[15,16]. Out of 203 FG main sequence stars observed with the Spitzer InfraRed Spectrometer (IRS), only two showed an excess in the short wavelength band (8.5–12 μm)[17].

To detect and characterize exozodiacal disks around a large number of sunlike stars *in the mid-IR*, significantly lower dust density levels must be accessed, and the HZ region needs to be spatially resolved from the star. This calls for improvements in both contrast and spatial resolution and means that long baseline / high accuracy (nulling) interferometry is required. Three ground-based instruments have tackled this observational challenge over the last 20 years: the Multi Mirror Telescope Nuller[18,19], the Keck Interferometer (KI) Nuller[20,21], and the Large Binocular Telescope Interferometer (LBTI)[22,23]. The KI observations reached a typical detection limit of ~300 to 500 zodis per star[24,25] between 8 and 10 μm. The LBTI exozodi key

science survey, which started in 2013[26,27] , has been demonstrating further improvements in sensitivity. The statistical analysis of LBTI data obtained to date indicates with 95% confidence that the typical (median) level of exozodi emission around sunlike stars with no outer cold dust reservoir previously known is below 26 zodis[28] . This number, which benefits from averaging over a few dozen stars, should not be confused with the detection limit *per individual star*, which is about 30 zodis for early spectral types and ~100-200 zodis for solar analogs.

While LBTI data indicate that the typical level of exozodiacal dust around sunlike stars is likely below the ~20 zodis confusion limit proposed by Defrere et al.[11], the LBTI detection limit *per individual* sunlike star is then still a factor of 10 above it. Limitations of this ground-based mid-IR approach must also be considered, such as bright thermal (sky) backgrounds and insufficient spatial resolution to resolve disk substructures. More importantly, basic dust properties (e.g., density profile and size distribution) cannot be uniquely derived from measurements over a wavelength range so narrow that either thermal emission or scattering completely dominates. This means that the brightness of exozodiacal emission at visible or shorter IR wavelengths cannot be reliably extrapolated from mid-IR measurements alone. This last issue is clearly illustrated by the intriguing detection of ~1% near-IR excesses around ~20% of main sequence stars,[29,30,31,32] with generally no detection counterpart in the mid-IR[33], pointing to populations of very hot and small (submicron) grains piling up close to the sublimation radius around these stars[33,34,35]. Visible exozodi observations are required[36] to measure the scattering phase function of dust grains, to better inform grain size and shape, and finally to enable connecting scattered light spectra with IR spectral energy distributions (SED) for compositional modeling. In short, to make further progress, high-contrast, high spatial resolution space-based observations are required, ideally at multiple wavelengths. The WFIRST CGI will start this journey, taking images and spectra of exozodiacal dust clouds at low dust density levels (~1-100 times solar), crossing an important threshold in debris disk physics, at a spatial resolution improved to ~50 mas in the visible.

4. HOW WILL CGI IMPROVE THE STATE OF KNOWLEDGE AND IMPACT FUTURE MISSIONS?

The benefits of using coronagraphy for the study of exoplanetary systems became clear with the first optical images of beta Pictoris's extended edge-on circumstellar disk obtained by Smith & Terrile[37] . Following the IRAS satellite discovery of a large IR excess around this star, these optical coronagraphic observations provided the first direct confirmation of planet formation and resolved images of dusty debris disks in another system. With the access to space provided by the Hubble Space Telescope (HST), many more circumstellar disks have been spatially resolved[38,39,40,41] since. However, HST's high contrast instruments have only achieved high levels of starlight suppression at large separations, such as the 10^{-9} flux ratio detection[42] of Fomalhaut b at 12″. The Space Telescope Imaging Spectrograph (STIS) is the only remaining operational high dynamic range optical instrument in space today. HST/STIS does provide access to separations as small as 0.25" in the visible, but only at ~10^{-4} contrast[43] , limiting exozodiacal observations to the closest stars and again to disks with very high surface brightness, typically 10^4 higher than in the solar system case (V-band surface brightness of ~23 mag/arcsec^2 at 1 AU).

With currently predicted point source detection limits better than 1.5×10^{-9} for angular separations ranging from 0.15" to 1.46", and at wavelengths ranging from 575 nm to 825 nm (Table 1), the WFIRST CGI promises a drastic improvement in high-contrast astronomical imaging capabilities at optical wavelengths. At 575 nm, the point source detection limit of 1.5×10^{-9} is expected to be reached as close as 150 mas from the star, a separation referred to hereafter as the coronagraph inner working angle (IWA). In comparison, radiometric calculations[44] indicate that for a solar system zodiacal cloud analog seen around a sunlike star at 7 pc at 575 nm and viewed under a 60 deg inclination with a 2.4m telescope, the disk flux contributed per spatial resolution element at the IWA (~1 AU in that case) is about 5×10^{-10} relative to the star. For a sunlike star at 7 pc, the CGI detection limit hence corresponds to ($1.5 \times 10^{-9} / 5\times10^{-10}$) = 3 zodis at 1 AU. Assuming the same instrument contrast at both separations and a quadratic fall-off in dust density, it would degrade to ~12 zodis at 2 AU. For sunlike stars located at a distance d < ~20 pc, i.e., close enough that some of their exozodiacal cloud emission can be captured outside of the CGI 150 mas IWA, the dust surface brightness at the physical IWA will decrease as $1/d^2$, like stellar flux. This means that for all sunlike stars within ~20 pc, the minimum dust-to-star flux ratio detectable per resolution element will stay the same. The best CGI sensitivity will always be reached at the 0.15" IWA, i.e., at a physical separation of 1AU*(d/7pc), and will be a constant 3 zodis. For cooler (hotter) stars than the Sun[45], the exozodi surface brightness at the Earth equivalent insulation distance would be lower (higher), and the detection limits in zodi units would be slightly worse (better). Figure 3 shows an illustration of the exozodiacal dust disk image expected when observing a nearby sunlike star with only 10 zodis of dust with the CGI hybrid Lyot coronagraph (HLC) mask at 575 nm. Dust emission at that level is clearly detected in a couple hours, together with some of the ring structures expected to be created by in-spiraling dust trapped in resonance with the orbit of a hypothetical perturbing planet.

Table 1: List of currently planned WFIRST/CGI filters and observing modes, together with performance predictions based on current-lab results (Pred) for each. Point source detection limits indicate the flux (relative to the central star) of the dimmest point source that can be detected at 5σ or higher *anywhere* within the range of angular separations indicated. Only the observing modes form the 3 highlighted rows will be *fully* tested on the ground, but all filters and modes listed will be available for CGI observations.

CGI Filters	λ_{Center} (nm)	BW	Channel	Masks	Working Angle (λ/D)	Working Angle (")	Point Source Detection Limit (Pred)	Starlight Suppression Region
1	575	10%	Imager	HLC	3–9 λ/D	0.15–0.43"	1.5×10^{-9}	360°
2	660	18%	IFS	SPC	3–9 λ/D			130°
2	660	18%	Imager	SPC	3–9 λ/D			130°
3	760	18%	IFS	SPC	3–9 λ/D	0.20–0.56"	3.5×10^{-9}	130°
3	760	18%	Imager	SPC	3–9 λ/D			130°
4	825	10%	Imager	HLC	3–9 λ/D			360°
4	825	10%	IFS	HLC	3–9 λ/D			360°
4	825	10%	IFS	SPC disk	6.5–12 λ/D			360°
4	825	10%	Imager	SPC disk	6.5–12 λ/D	0.50–1.46"	6×10^{-10}	360°

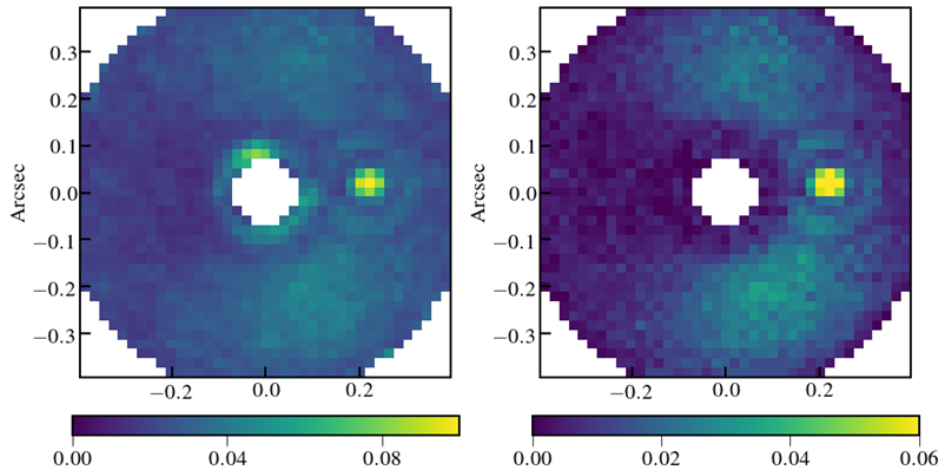

Figure 3: Simulated WFIRST CGI observations (HLC 575 nm imaging mask) of a nearby sunlike star (1 Ori, spectral type F6V at ~8 pc) hosting an exozodi dust cloud 10× denser than in the solar system, showing resonant structures due to a hypothetical Jovian planet located at 1.6 AU. The assumed instrument parameters are the current lab-validated performance of coronagraph wavefront control and detectors, and the detection limits listed in Table 1. Flux color scale indicated at the bottom is in units of photoelectrons/s and shown using a square-root stretch. Simulated exposure time is 2.8 h. (Courtesy of M. Rizzo, N. Zimmerman and the "Haystacks" team). The right image shows the contrast enhancement provided by PSF subtraction (speckle removal) using observations of a reference star. The field of view diameter is 0.8" in both images.

More detailed instrument simulations and disk observation DRMs will be required to better understand what debris disk physical properties can actually be extracted from CGI exozodi images and at what level of accuracy. Field-dependent variations in the coronagraph point spread function require accounting for the instrument response function before dust grain characteristics (e.g. size distribution and scattering function) are measured. In particular, and as illustrated in Figure 4, the off-axis PSF is broad and varies greatly around the IWA: it goes from a very asymmetric PSF inside the IWA, shifting the peak brightness position outward, to a better behaved PSF for sources located outside of the IWA.

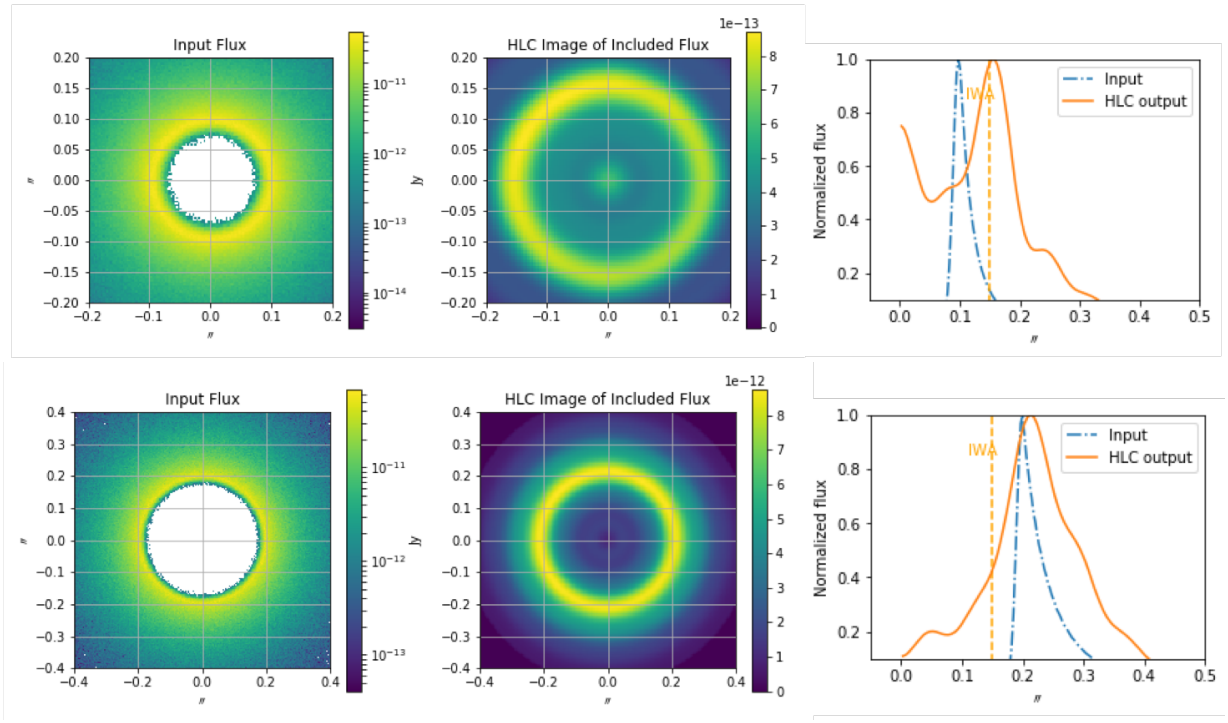

Figure 4: Noiseless simulations illustrating the effect of CGI (HLC) coronagraphic PSF variations close to the 0.15" inner working angle. From left to right: input disk model, coronagraphic image and comparison of the two normalized brightness distributions (radial cuts). Top panel: pole-on ring-like disk structure with a radius of 0.1", inside the IWA. Bottom panel: ring-like disk structure centered at 0.2", outside the IWA. Note the different angular scales between the top and bottom panels. In the inner ring case, most of the brightness distribution is pushed outwards, and some of the flux is sent to the very center. Credit: Ewan Douglas (MIT).

5. CONCLUSION

The simulation results shown in Figure 3 illustrate the power of conducting sensitive spatially resolved exozodiacal observations with the WFIRST CGI, searching at the same time for the presence of otherwise undetectable planets (early type stars), possibly constraining their mass and orbit via their resonant structures, or the clearing of the inner disk. CGI will offer the first opportunity to explore disk-planet interactions at low dust density levels (~3× solar using current best performance predictions), and at very small physical separations: within the snow-line of sunlike stars located within ~20 pc, and in the HZ of those closer than ~10 pc. This science case is very robust for 2 main reasons. First, the current best observations of exozodi disks around sunlike stars[28] show detection limits of the order of 100 zodis or more, which can be reached even if CGI were only to perform at its minimum performance level (BTRs). Second, -and conversely to the case of mature planets which have visible contrast levels limited to 10^{-8} even for the largest planets-, debris disks come with a broad continuum of dust opacity levels, surface brightness and flux ratios. In addition, CGI will directly measure exozodi levels and resolve their spatial structures at the visible wavelengths considered for future missions for the first time. These observations will start to establish whether the zodiacal cloud of our inner solar system is representative of the population of our nearest sunlike neighbors; such visible observations cannot be obtained from the ground. The CGI will hence pave the way to even more capable future direct imaging missions, as illustrated by the ongoing Starshade Probe, HabEx, and LUVOIR concept studies.

ACKNOWLEDGEMENTS

Part of this research was carried out at the Jet Propulsion Laboratory, California Institute of Technology, under a contract with the National Aeronautics and Space Administration. Support for part of this work was provided by the WFIRST Science Investigation teams prime awards #NNG16PJ24C and #NNX15AK69G.

REFERENCES

[1] Kelsall, T. et al. 1998, ApJ 508, 44
[2] Fixsen & Dwek 2002, ApJ 578, 1009
[3] Roberge, A. et al. 2017, PASP 129, 124401
[4] Nesvorny D., et al. 2010, ApJ 713, 816
[5] Backman, D.E. & Paresce, F. 1993, Protostars and Planets III, 253
[6] Gomes, R. et al. 2005, Nature 435, 346
[7] Mennesson, B. & Mariotti, J.M. 1997, Icarus, 128, 202
[8] Defrere, D. et al. 2010, A&A 509, 9
[9] Roberge, A. et al. 2012, PASP 124, 799
[10] Stark C. et al. 2015a, ApJ 808, 149
[11] Defrere, D. et al. 2012, SPIE 8442
[12] Stark, C. et al. 2011, AJ 142, 123
[13] Stark, C. et al. 2015b, ApJ 801, 128
[14] Beichman, C. & Velusamy, T. 1997, AAS meeting 191, 29, 1310
[15] Beichman, C. et al. 2006, ApJ 639, 1166
[16] Bryden, G. et al. 2006, ApJ 636, 1098
[17] Lawler, S. et al. 2009, ApJ 705, 89
[18] Hinz, P. et al. 1998, Nature 395, 251
[19] Liu et al. 2009, ApJ 693, 1500
[20] Colavita, M. M. et al. 2009, PASP 121, 1120
[21] Serabyn, E. et al. 2012, ApJ 748, 55
[22] Hinz, P. et al. 2014, SPIE 9146
[23] Defrere, D. et al. 2016, ApJ 824, 66
[24] Millan-Gabet et al, R. 2011, ApJ 734, 67
[25] Mennesson, B. et al. 2014, ApJ 797, 119
[26] Hinz, P. et al. 2016, SPIE Conf. Proc 9907
[27] Weinberger, A. et al. 2015, ApJS, 216, 24
[28] Ertel, S. et al, 2018, AJ, 155, 194
[29] Absil et al. 2006, A&A, 452, 237
[30] Akeson et al. 2009, ApJ, 691, 1896
[31] Absil et al. 2013, A&A, 487, 1041
[32] Ertel, S. et al, 2014, A&A 570, 128
[33] Mennesson, B. et al. 2011, ApJ 736, 14
[34] Lebreton, J. et al. 2013, A&A 555, 146

[35] Kirchschlager, S. et al. 2017, MNRAS 467, 1614
[36] Kral. Q. et al. 2017, AstRv 13, 69
[37] Smith, B.A. & Terrile, R.J. 1984, Sci 226, 1421
[38] Clampin, M. et al. 2003, AJ 126, 385
[39] Boccaletti, A. et al 2003, ApJ 585, 494
[40] Ardila, D. et al. 2004, ApJ, 617, 147
[41] Krist, J. et al. 2005, AJ 129, 1008
[42] Kalas, P. et al. 2008, Sci 322, 1345
[43] Debes, J. et al. 2016, JATIS, 2
[44] Roberge, A. et al. 2012, PASP, 124, 799
[45] Stark, C. et al. 2014, ApJ 795, 122
[46] Douglas, E. S. et al. 2018, SPIE Conf. Proc 10705